



Cite this: *RSC Adv.*, 2021, 11, 13486

# Specific adsorption and determination of aspartame in soft drinks with a zein magnetic molecularly imprinted modified MGCE sensor†

Ling Tan,<sup>ac</sup> Qing-Yao Li,<sup>‡a</sup> Yan-Jun Li,<sup>a</sup> Rong-Rong Ma,<sup>a</sup> Jia-Yuan He,<sup>a</sup> Zhuang-Fei Jiang,<sup>a</sup> Li-Li Yang,<sup>a</sup> Chong-Zhi Wang,<sup>d</sup> Ling Luo,<sup>\*b</sup> Qi-Hui Zhang <sup>\*ad</sup> and Chun-Su Yuan<sup>d</sup>

In this work, an efficient and sensitive magnetic molecularly imprinted polymer with zein and deep eutectic solvents (ZDM-MIPs) was designed and synthesized to exclusively adsorb and detect aspartame (ASP). We used zein, together with deep eutectic solvents (DESs) and Fe<sub>3</sub>O<sub>4</sub> as the cross-linker, functional monomer and support material, respectively. A magnetic glassy carbon electrode (MGCE) modified with ZDM-MIPs was used for selective recognition of ASP. The electrochemical response of the ZDM-MIPs-MGCE for quantification of ASP was evaluated with a portable electrochemical detection station with differential pulse voltammetry and cyclic voltammetry. The responses of ZDM-MIPs-MGCE signified a good linear relationship with ASP concentrations in the range of 0.1–50 µg mL<sup>-1</sup>. The sensor systems showed good accuracy and precision, with recovery percentages between 84% and 107%. These results suggested that the obtained ZDM-MIPs exhibited good adsorption performance for ASP in soft drinks, and this method could be used to determine ASP content in actual food samples.

Received 25th December 2020

Accepted 31st March 2021

DOI: 10.1039/d0ra10824c

rsc.li/rsc-advances

## 1. Introduction

Aspartame (L-aspartyl-L-phenylalanine methyl ester; ASP) has been widely used in the food industry as an alternative to sugar.<sup>1</sup> To decrease sugar and caloric content, the food industry uses artificial sweeteners to produce a variety of foodstuffs, including powdered drinks, chewing gum, and jellies.<sup>2</sup> However, some animal studies have indicated that ASP is a carcinogenic agent in mice.<sup>3,4</sup> Because the effects of ASP on human health continue to be controversial,<sup>5</sup> the acceptable daily intake of ASP is recommended not to exceed 40 mg kg<sup>-1</sup> of body weight.<sup>6</sup> Therefore, the developing an assay for the accurate and sensitive determination of this artificial sweetener in food is essential.

Various technologies have been developed to determine ASP, such as high-performance liquid chromatography (HPLC),<sup>7</sup> mass spectrometry (MS)<sup>8</sup> and electrochemical analysis.<sup>9</sup> Among them, electrochemical analysis is regarded as one of the most

promising methods for the determination of ASP. Electrochemical methods offer many advantages for tracking analytes, because of their relatively low cost and short analysis time.<sup>10,11</sup> A magnetic glassy carbon electrode (MGCE) is among the widely used electrodes,<sup>12</sup> such as for the analysis and detection of pigments, drugs, proteins and organic pollutants.<sup>13–15</sup> MGCE has several advantages, including good electrical conductivity, high chemical stability, a low thermal expansion coefficient, hard texture, good air tightness, and a broad application potential (approximately –1 to 1 V relative to a saturated calomel electrode).<sup>14</sup> MGCE is increasingly being used in electrochemical and electroanalytical chemistry experiments.<sup>15</sup> The newly developed portable electrochemical workstations also have many favorable characteristics, such as small size and portability. Similarly, the portable electrochemical workstations can perform various electrochemical techniques such as cyclic voltammetry (CV) and differential pulse voltammetry (DPV), thus meaning the different requirements of electricity chemical measurements. The combined use of MGCE and portable electrochemical workstations can greatly increase the range of application and portability. However, the interfering substances in the actual samples can affect the accuracy of the method. Therefore, it is necessary to selectively detect ASP.

Molecularly imprinted polymers (MIPs) with specific binding sites exhibit ultrahigh selectivity for template molecules or ions, and are recognized as synthetic antibody mimics.<sup>16</sup> Compared to other absorbents, MIPs have the advantage of easy preparation, high specificity, and broad adaptability.<sup>17,18</sup> Therefore,

<sup>a</sup>School of Chemistry and Chemical Engineering, Chongqing University, Chongqing 400044, China. E-mail: qhzhong@cqu.edu.cn; Fax: +86-023-65102531

<sup>b</sup>Chongqing Cancer Institute, Chongqing Cancer Hospital, Chongqing University Cancer Hospital, Chongqing, 400030, China. E-mail: ling.luo.cqch@hotmail.com; Fax: +86-023-65311341

<sup>c</sup>School of Pharmaceutical Sciences, Chongqing University, Chongqing, 400044, China

<sup>d</sup>Tang Center for Herbal Medicine Research, Department of Anesthesia & Critical Care, University of Chicago, Chicago, IL 60637, USA

† Electronic supplementary information (ESI) available. See DOI: 10.1039/d0ra10824c

‡ Co-first author: these authors contributed equally to the article.



MIPs are widely used in a variety of areas, including separation science, solid phase extraction, and sensors.<sup>19–21</sup> However, with the traditional molecular imprinting method, the most recognition sites of the obtained polymers are embedded in the interior of the MIPs, thus decreasing the recognition sites in the material and the binding ability. Surface imprinting technology has been demonstrated to overcome these problems. Furthermore, common support materials often include SiO<sub>2</sub>, TiO<sub>2</sub>, carbon materials, and magnetic materials.<sup>22–24</sup> Among them, Fe<sub>3</sub>O<sub>4</sub> nanoparticles have been widely used in the synthesis of MIPs,<sup>25</sup> owing to their advantages of simple preparation, sensitivity, rapid separation, and low cost. Magnetic MIPs (MMIPs) with Fe<sub>3</sub>O<sub>4</sub> nanoparticles as the core material provide good magnetic response and strong electrochemical signal for the polymer.<sup>26</sup> And under the action of a magnetic field, the magnetic molecularly imprinted polymer is easily separated from the sample solution, without filtering or centrifugation.

Unfortunately, the large amounts of organic solvents used in the synthesis are not consistent with the idea of green chemistry. In addition, the materials used to detect analytes in food samples should be non-toxic and environmentally friendly. Deep eutectic solvents (DESSs) can be attained by heating a mixture of hydrogen bond acceptor (HBA) and a metal salt or hydrogen bond donor (HBD) in a proper ratio.<sup>27</sup> DESSs are new types of organic or pseudo-organic ionic liquids with merits such as non-toxicity, biocompatibility and so on. Consequently, DESSs were applied to the synthesis of MIPs to improve the selectivity of MIPs. Zein is a mixture of proteins with an average molecular weight of 25 000 to 45 000, which can be classified into  $\alpha$ -,  $\beta$ -,  $\gamma$ -, and  $\delta$ -zein according to solubility and amino acid sequence homology.<sup>28,29</sup> It is hydrogen-bonded to the imino group in the main chain of the peptide and has unique film-forming property, biodegradability, and biocompatibility.<sup>30,31</sup> Therefore, zein has many potential applications in the food and pharmaceutical industries.

In this study, we described novel zein magnetic MIPs (ZDM-MIPs), which were successfully prepared with ASP as an imprinted template. DESSs were used as functional monomers, and zein was used as the cross-linker. Biocompatible zein is non-toxic, and DESSs can provide hydrogen bond acceptors and donors to improve the selectivity of polymers. After removal of the template molecule ASP, ZDM-MIPs were obtained and combined. Using portable electrochemical workstations with an electrochemical detection method, we successfully detected ASP in complex samples. Finally, we investigated and discussed the specific capture performance of the material, such as the binding kinetics, equilibrium, and selectivity.

## 2. Materials and methods

### 2.1 Reagents

Aspartame (>99%), acesulfame potassium (>99%), glycyrrhizin acid (>99%) and zein were purchased from Nanjing Puyi Biological Technology Co. Ltd (Jiangsu China). Iron(III) chloride hexahydrate (FeCl<sub>3</sub>·6H<sub>2</sub>O), ethylene glycol (EG), sodium acetate anhydrous (NaAc), ethanol and sodium citrate (Na<sub>3</sub>Cit·2H<sub>2</sub>O) were purchased from Chengdu Kelong Chemical Co. Ltd

(Chengdu, China). Potassium ferricyanide (K<sub>3</sub>[Fe(CN)<sub>6</sub>]) was obtained from Tianjin Zhiyuan Chemical Reagent Co. Ltd (Tianjin, China). All reagents were analytical reagent grade and water used in the experiments was double distilled.

### 2.2 Apparatus

A scanning electron microscope (SEM, Japan Electronics JEM-2100F, Japan) and transmission electron microscopy (TEM, Zeiss ultra-high resolution thermal field electron microscope, Germany) were used to characterize the morphology of materials. The infrared spectrum (4000–400 cm<sup>−1</sup>) was recorded on a Fourier-transform infrared spectrometer (FT-IR, Nicolet 6700, Thermo Nicolet Co. Waltham, MA, USA). A thermogravimetric analysis (TGA) was carried out from 25 to 800 °C with a heating rate of 10 °C min<sup>−1</sup> under air environment (TGA/DSC1/1600LF, Mettler-Toledo, Switzerland). Magnetization was measured at room temperature using a vibrating sample magnetometer (VSM, MicroSense-EZ9, USA).

The concentration of ASP was detected by HPLC (Agilent Technologies, Santa Clara, CA, USA) with C<sub>18</sub> (Agilent, 250 × 4.6 mm, Agilent Technologies) at a mobile phase flow rate of 0.6 mL min<sup>−1</sup>. The mobile phase for ASP determination was 0.05% phosphoric acid/methanol (40 : 60, v/v) at 25 °C. The UV detector spectra was set at 210 nm.

### 2.3 Synthesis of ZDM-MIPs and ZDM-NIPs materials

**2.3.1 Synthesis of DESSs.** Deep eutectic solvents (DESSs) were prepared according to the method previously used by our group. Briefly, choline chloride, caffeic acid, and formic acid (molar ratio 1 : 6 : 3) were added to the flask and stirred at 90 °C for one hour, until homogeneous liquid formed.

**2.3.2 Prepare Fe<sub>3</sub>O<sub>4</sub> nanoparticles.** The spherical Fe<sub>3</sub>O<sub>4</sub> nanoparticles were synthesized by solvothermal method according to the literature.<sup>32</sup> In a general synthesis, 5.4 g FeCl<sub>3</sub>·6H<sub>2</sub>O was dissolved in 160 mL ethylene glycol under alternate magnetic stirring and ultrasonic dispersion at room temperature. Then, 12.4 g sodium acetate anhydrous and 1.6 g sodium citrate were added to the orange solution. The mixture was heated under magnetic stirring at 150 °C, until a uniform dark brown solution was formed. The solution was transferred into a Teflon lined stainless steel autoclave to be heated at 200 °C for 8 h. After cooling to room temperature, Fe<sub>3</sub>O<sub>4</sub> microspheres were separated magnetically and washed with water and ethanol 3 times and then dried under vacuum overnight.

**2.3.3 Prepare ZDM-MIPs and ZDM-NIPs.** ZDM-MIPs were prepared based on the self-polymerization ability of zein in water. In this procedure, Fe<sub>3</sub>O<sub>4</sub>, DESSs and zein were used as support material, functional monomer and crosslinking agent, respectively. The preparation process was as follows: ASP (145 mg), DESSs (1 mL), and 70% ethanol–water (50 mL) were added to a flat-bottomed flask for pre-polymerization for 18 h. Then Fe<sub>3</sub>O<sub>4</sub> (200 mg) and zein (250 mg) were added and sonicated for 30 min. After ultrasonic processing, the mixed solution was shaken in a constant temperature shaker for 12 h. Then the solid was separated by a magnet, washed three times with 70%



ethanol–water and then 30 mL of distilled water was added and self-polymerized for 8 hours. After the reaction, the MMIPs were washed with methanol–HAc (9 : 1, v/v) to remove the template of ASP. Finally, the product was washed to neutral with double distilled water, and then dried at 45 °C overnight. As a control, magnetic non-imprinted polymers with zein and deep eutectic solvents (ZDM-NIPs) were prepared using the same process only without the addition of the template of ASP.

## 2.4 Preparation of imprinted sensor and electrochemical measurement

The magnetic glassy carbon electrode (MGCE) was polished with  $\text{Al}_2\text{O}_3$  and then rinsed thoroughly with ultra-pure water. Subsequently, the polished MGCE was ultra-sonicated for 5 min in ethanol, then 5 min in ultra-pure water, and finally was blown dry in air. After drying in air, 15  $\mu\text{L}$  of a 1.5  $\text{mg mL}^{-1}$  ZDM-MIPs suspension was dropped onto the MGCE, and the modified electrode was dried at room temperature.

CV measurements were taken from  $-0.2$  V to  $0.7$  V at a scan rate of  $50 \text{ mV s}^{-1}$ . Electrochemical measurements were carried out in a 30 mL aqueous solution containing  $5.0 \text{ mmol L}^{-1}$  of  $\text{K}_3[\text{Fe}(\text{CN})_6]$  and  $0.2 \text{ mol L}^{-1}$  of KCl at room temperature.

DPV measurements were taken from  $-0.2$  V to  $0.4$  V, the potential increment was  $0.004$  V, the pulse width was  $0.05$  V, the pulse amplitude was  $0.05$  V, and the pulse interval was  $0.1$  s.

## 2.5 Adsorption experiments

To investigate the adsorption properties of ZDM-MIPs, we performed kinetic adsorption, static adsorption and selective adsorption experiments.

In the kinetic experiments, 10.0 mg ZDM-MIPs or ZDM-NIPs was added to a centrifuge tube, which contained 5.0 mL of ASP standard solutions (with a concentration of  $100 \mu\text{g mL}^{-1}$ ). The mixtures were shaken in a thermostatic oscillator at  $25^\circ\text{C}$  at 105 rpm. Samples were obtained at 5, 10, 20, 40, 60, 90, and 120 min and the concentration of ASP in the supernatant was detected by HPLC at 210 nm. The adsorption amount ( $Q$ ,  $\text{mg g}^{-1}$ ) was calculated by the following equation.

$$Q = (C_0 - C_e)V/m \quad (1)$$

where  $Q$  ( $\text{mg g}^{-1}$ ) is the adsorption amount.  $C_0$  ( $\mu\text{g mL}^{-1}$ ) and  $C_e$  ( $\mu\text{g mL}^{-1}$ ) are the initial and equilibrium concentrations of ASP.  $V$  (mL) and  $m$  (mg) are the volume of solution and the mass of sorbents, respectively.

For static adsorption experiments, 10.0 mg of ZDM-MIPs or ZDM-NIPs was added to 5.0 mL of a series of ASP methanol solutions with concentrations ranging from 10 to  $300 \mu\text{g mL}^{-1}$ . The mixture was shaken for 120 min as described above. The adsorption capacity was calculated in the same way as that of dynamic adsorption.

For selective adsorption, acesulfame and glycyrrhizin acid were selected as similar substances to evaluate the selective adsorption properties of ZDM-MIPs (or ZDM-NIPs). 10.0 mg of ZDM-MIPs or ZDM-NIPs was added to the mixture solution containing  $100 \mu\text{g mL}^{-1}$  aspartame, acesulfame and

glycyrrhizin acid standard solutions and shaken for 2 h. The concentration of the supernatant was then detected by HPLC.

## 2.6 Sample analysis

**2.6.1 Remove ASP in commercial soft drinks.** In this experiment, we prepared a simple straw to separate ASP from commercial soft drinks. Preparation of sample solution: ultra-sonically degassed the commercial soft drinks at room temperature for 30 minutes, then added a certain amount of ASP standard solution, and then diluted the resulting solution 20 times with distilled water to obtain a sample solution. 100 mg of ZDM-MIPs material was placed in the middle of the sucker and the sucker was then inserted into the sample solution containing ASP. After adsorbing, the target substance ASP was adsorbed onto the surface of the ZDM-MIPs. The solution after adsorption was determined by HPLC to determine the concentration of ASP. The detection conditions were as described above. The analysis of each group was repeated three times ( $n = 3$ ).

**2.6.2 Application of ZDM-MIPs to drinks samples.** Recovery tests for ASP in samples were investigated. The soft drink samples were degassed in an ultrasonic bath for 30 min at room temperature, and then spiked with known concentrations of  $40$ – $400 \mu\text{g mL}^{-1}$  ASP standard solutions. The resulting mixed solutions were diluted 80 times with distilled water, and then filtered through a  $0.45 \mu\text{m}$  nylon membrane to obtain clear test samples, which were examined by the DPV method.

# 3. Results and discussion

## 3.1 Preparation of ZDM-MIPs

Fig. 1 showed the synthesis process of ZDM-MIPs. First,  $\text{Fe}_3\text{O}_4$  nanoparticles were used as support material, and the molecularly imprinted layer was synthesized on the surfaces of  $\text{Fe}_3\text{O}_4$  nanoparticles. In the synthesis procedure, DESs acted as the functional monomer, ASP acted as the template molecule, and zein acted as the cross-linker. The molecularly imprinted layer was polymerized on the  $\text{Fe}_3\text{O}_4$  nanoparticles through the self-assembly of zein. In this research, the innovation of ZDM-MIPs lies in the application of DESs and zein. DESs are novel, non-toxic and environmentally friendly solvents that can be used to replace other functional monomers, such as methacrylic acid (MAA), in the preparation of polymers. In the polymerization procedure, functional monomer DESs can provide hydrogen bond donors and hydrogen bond acceptors, so DESs can interact with the  $-\text{COOH}$  and  $-\text{NH}_2$  groups of aspartame through hydrogen bonding. Zein is an inexpensive and biodegradable plant protein, which is used as a molecularly imprinted cross-linker on the basis of its self-polymerization in water. Finally, magnetic ZDM-MIPs were assembled after being washed with a solution of methanol and acetic acid (9 : 1, v/v) to remove the template molecules. After molecular imprinting, ZDM-MIPs have binding sites that can match the template molecule (ASP). The current response of ZDM-MIPs glassy carbon electrode sensor was reduced after ASP recognition because the specific binding of ASP to the imprinted cavities



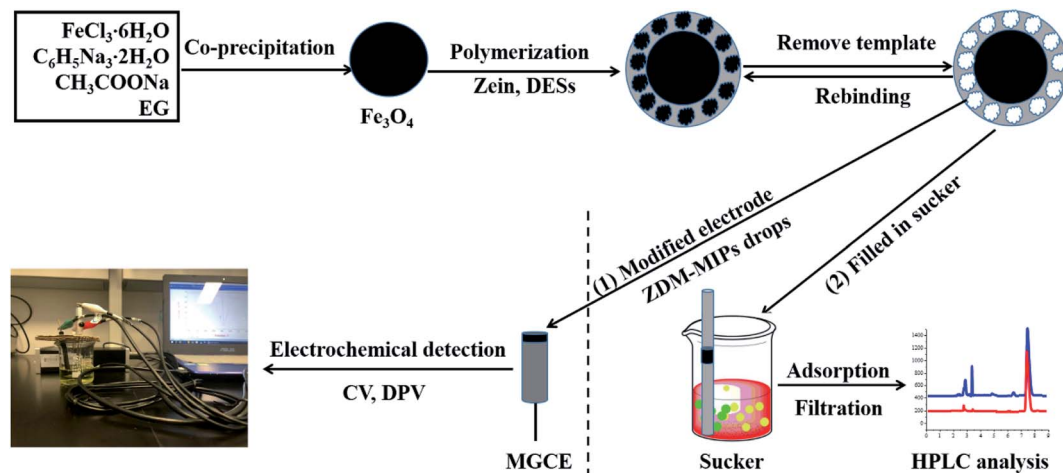


Fig. 1 Schematic representation of the synthesis procedure of ZDM-MIPs.

blocked the electron transfer of the electrode. The magnitude of the peak current reduction was related to the number of target molecules captured by the molecularly imprinted polymer.

In this work, we determined the solubility characteristics of zein in different ethanol concentrations allowing zein to form a film on the surface of the magnetic material. Therefore, the solvents used in the molecularly imprinted synthesis were highly important. We tested different concentrations of ethanol–water solutions and calculated the adsorption amounts of the synthesized molecularly imprinted materials. We

determined that 70% ethanol solution as the solvent was optimal for the synthesis of ZDM-MIPs (Fig. S1A†), because it resulted in the highest adsorption, in agreement with findings in other reports.

Zein was used as a cross-linking agent, and its amount was determined according to the adsorption properties of the synthetic material. The effects of different amounts of zein on synthetic materials were investigated, and the optimum amount of zein was found to be 250 mg (Fig. S1B†). The amount of adsorption of the material decreased with an excess zein,

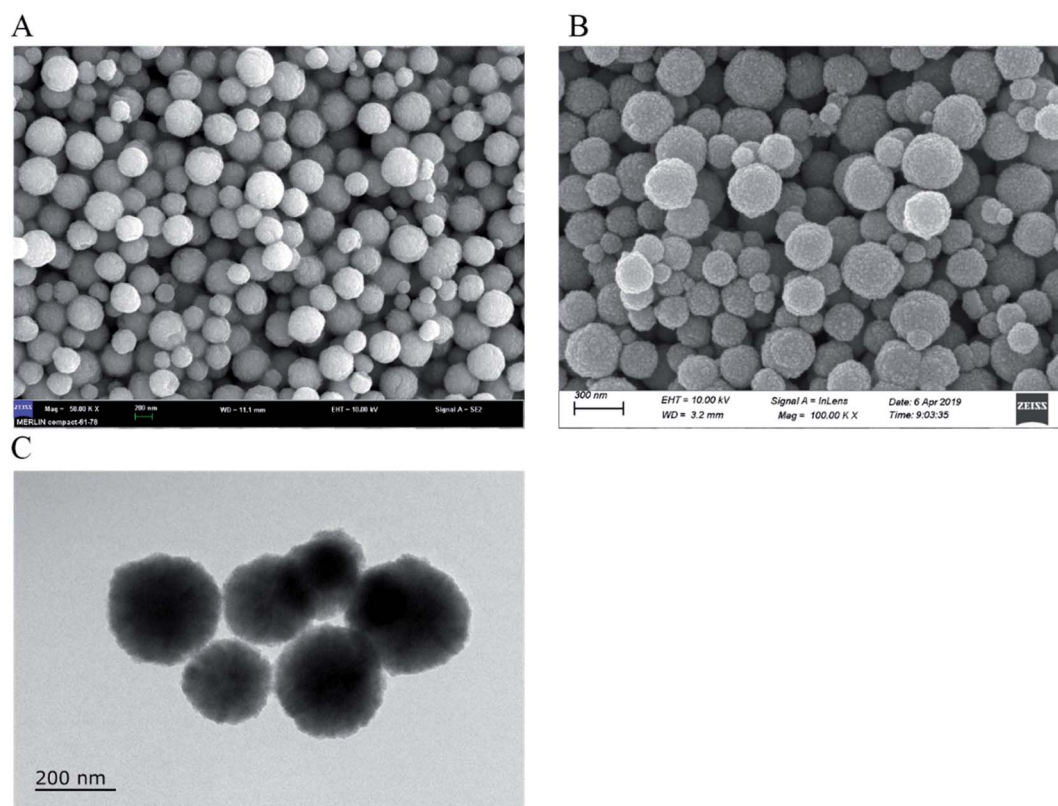


Fig. 2 SEM images of (A)  $\text{Fe}_3\text{O}_4$ , (B) ZDM-MIPs, and (C) TEM images of ZDM-MIPs.



possibly because excess zein caused excessive polymerization and decreased the number of binding sites.<sup>33</sup>

In this study, DESs were the functional monomer of the ZDM-MIPs. The amount of DESs was an essential parameter to the performance of ZDM-MIPs, which had been investigated to prepare the best ZDM-MIPs. To improve the adsorption capacity of the ZDM-MIPs, we also investigated the effects of the amount of DESs according to the adsorption  $Q$  value and found that the optimized amount of DESs was 2 mL (Fig. S1C†). Lacking DESs can't provide enough multiple interactions between the functional monomer and template molecule, but too much DESs will form a thicker polymer layer, thus blocking the imprinted cavities. 2 mL was selected as the most suitable amount because the maximum adsorption capacity of ZDM-MIPs was obtained.

### 3.2 Characterization

**3.2.1 Morphological structural characterization of ZDM-MIPs.** The morphological structures of  $\text{Fe}_3\text{O}_4$  and ZDM-MIPs were observed through SEM and TEM (Fig. 2). As shown in Fig. 2A, the  $\text{Fe}_3\text{O}_4$  nanoparticles were smooth and monodisperse microspheres with uniform sizes of approximately 250 nm. After molecular imprinting, the ZDM-MIPs exhibited a relatively spherical structure, good dispersion and small diameter of 300–450 nm. The surface of ZDM-MIPs was larger and rougher than that of  $\text{Fe}_3\text{O}_4$  magnetic nanoparticles (Fig. 2B). The TEM image of ZDM-MIPs (Fig. 2C) clearly showed that its diameter increased to approximately 300 nm and layers

(gray) surrounding the surfaces of the  $\text{Fe}_3\text{O}_4$  nanoparticles (black), thus indicating that the molecularly imprinted thin film has been successfully synthesized on the  $\text{Fe}_3\text{O}_4$  nanoparticles. The obtained ZDM-MIPs materials with core-shell structures and uniform particle size suggested that the preparation of the molecularly imprinted layer was successful.

**3.2.2 FT-IR characterization.** In this study, FT-IR spectroscopy was employed to prove the successful preparation of ZDM-MIPs. Fig. 3A showed the FT-IR spectra of zein,  $\text{Fe}_3\text{O}_4$ , and ZDM-MIPs. For  $\text{Fe}_3\text{O}_4$ , the strong absorption peak at  $577\text{ cm}^{-1}$  was attributed to the characteristic peak of the Fe–O bond stretching vibration,<sup>34</sup> indicating the successful synthesis of  $\text{Fe}_3\text{O}_4$ . For zein, the adsorption peak at  $1238\text{ cm}^{-1}$  was assigned to the stretching vibration of C–OH in aromatic rings. The absorption peak at  $1644\text{ cm}^{-1}$  was assigned to the C=O stretching vibration of amide I groups.<sup>35</sup> And the peak at  $1543\text{ cm}^{-1}$  was attributed to the C–N stretching vibration and N–H bending of amide II groups in zein.<sup>36</sup> The adsorption peak of  $2928\text{ cm}^{-1}$  was assigned to the C–H bond stretching vibration.<sup>37</sup> The spectra of ZDM-MIPs had peaks similar to the major peaks of zein and  $\text{Fe}_3\text{O}_4$ , thus demonstrating the successful synthesis of ZDM-MIPs.

**3.2.3 TGA analysis.** TGA was used to further study the heat stability of the ZDM-MIPs nanoparticles. The thermogravimetric curve was shown in Fig. 3B. With the temperature increasing from  $25^\circ\text{C}$  to  $100^\circ\text{C}$ , the mass loss of ZDM-MIPs was approximately 5%, owing to the loss of free moisture and

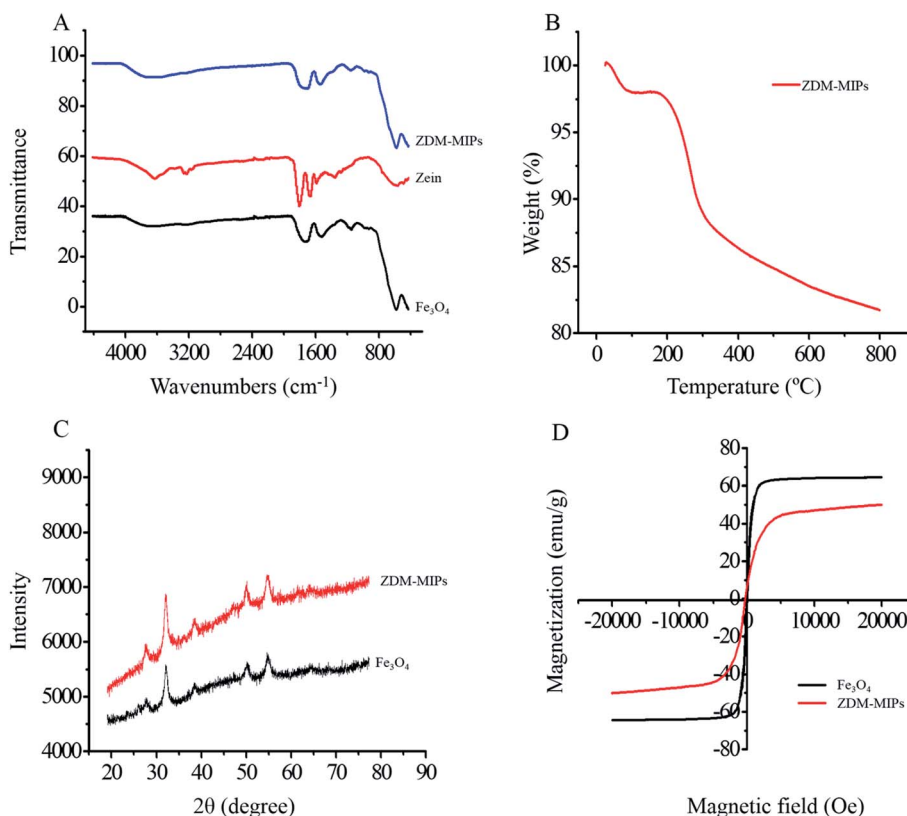


Fig. 3 (A) The FT-IR spectra of  $\text{Fe}_3\text{O}_4$ , Zein, and ZDM-MIPs (B) the thermogram of synthesized ZDM-MIPs, (C) XRD patterns of the  $\text{Fe}_3\text{O}_4$  and ZDM-MIPs, and (D) the magnetic properties investigation of ZDM-MIPs.



physically bound moisture in the materials. When the temperature rose to 800 °C, the organic components on the surfaces of the ZDM-MIPs decomposed, and the mass loss of the ZDM-MIPs was approximately 15%. Thus, the ZDM-MIPs appeared to have good thermal stability.

**3.2.4 X-ray diffraction analysis.** XRD analysis was performed to investigate the crystal structures of  $\text{Fe}_3\text{O}_4$  and ZDM-MIPs. Fig. 3C showed the XRD patterns of the  $\text{Fe}_3\text{O}_4$  and ZDM-MIPs. In the  $2\theta$  range of 20–90°, six characteristics diffraction peaks of  $\text{Fe}_3\text{O}_4$  were observed in Fig. 3C. They were indexed as (220), (311), (400), (422), (511), and (440) planes of  $\text{Fe}_3\text{O}_4$  crystal. From the XRD patterns of ZDM-MIPs, it can be seen that the six characteristic diffraction peaks of  $\text{Fe}_3\text{O}_4$  still existed. These observations confirmed that the crystalline structure of  $\text{Fe}_3\text{O}_4$  didn't change after being coated with molecularly imprinted polymers.<sup>27</sup>

**3.2.5 Vibrating sample magnetometry analysis.** In this study, the magnetic properties of the synthetic  $\text{Fe}_3\text{O}_4$  and ZDM-

MIPs were characterized by VSM. Fig. 3D showed the magnetization curves of  $\text{Fe}_3\text{O}_4$  and ZDM-MIPs. The saturation magnetization values of  $\text{Fe}_3\text{O}_4$  and ZDM-MIPs were 64.41  $\text{emu g}^{-1}$  and 48.84  $\text{emu g}^{-1}$ , respectively. The saturation magnetization of the ZDM-MIPs was lower than that of  $\text{Fe}_3\text{O}_4$  because the molecularly imprinted layers were synthesized on the surfaces of  $\text{Fe}_3\text{O}_4$ . Although the  $\text{Fe}_3\text{O}_4$  surfaces were coated with molecularly imprinted layers, they still could be separated quickly with an external magnetic field. This was consistent with related literature reports.<sup>38</sup> Therefore, the prepared ZDM-MIPs possessed strong magnetism to ensure that particles could be separated rapidly from the sample solution.

### 3.3 Adsorption performance of ZDM-MIPs

**3.3.1 Adsorption kinetics.** The adsorption kinetics of ASP on ZDM-MIPs and ZDM-NIPs were shown in Fig. 4A. In the first 20 min, the adsorption amount of ZDM-MIPs increased rapidly

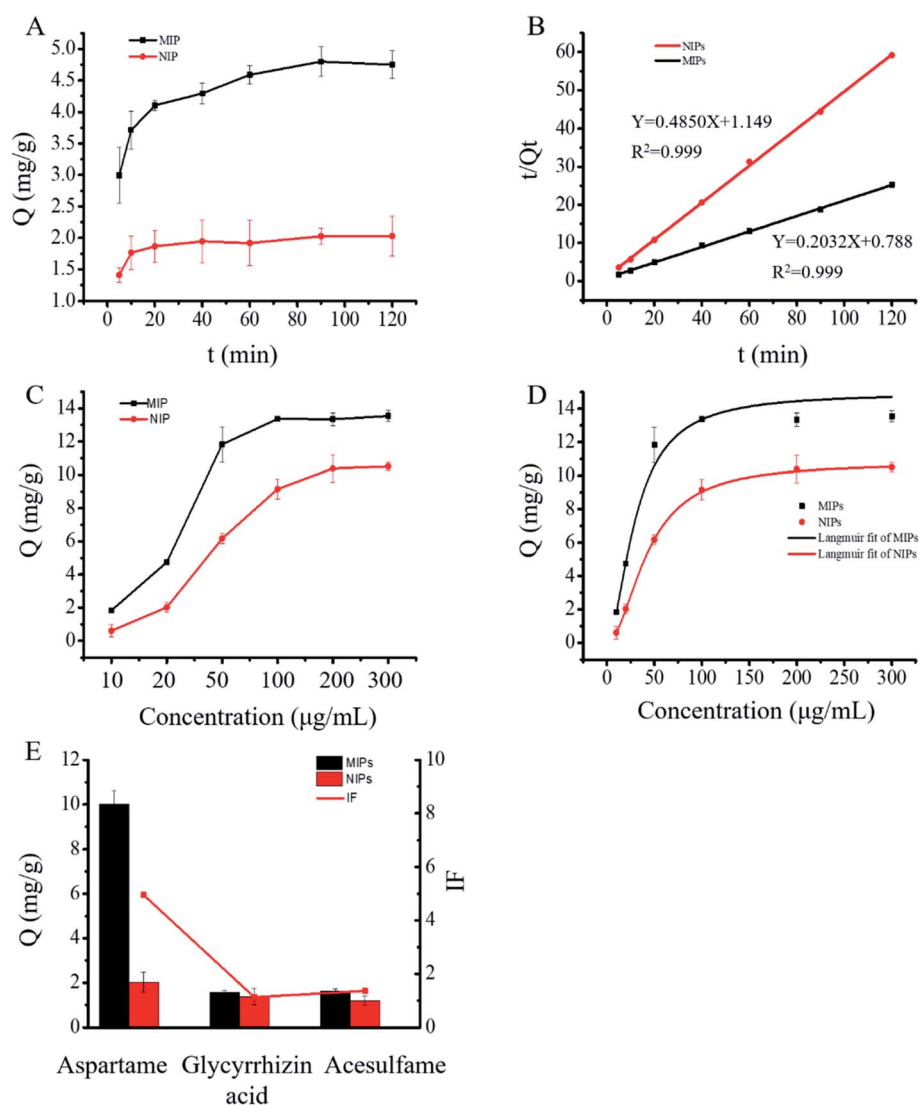


Fig. 4 (A) Characteristic adsorption kinetic of ZDM-MIPs and ZDM-NIPs, (B) pseudo-second-order equation of ZDM-MIPs and ZDM-NIPs, (C) characteristic adsorption isotherms of ZDM-MIPs and ZDM-NIPs, (D) Langmuir isotherm models and Freundlich isotherm models of ZDM-MIPs and ZDM-NIPs, (E) selective adsorptions of ZDM-MIPs and ZDM-NIPs on aspartame, glycyrrhizin acid, and acesulfame.

and gradually reached equilibrium within 90 min. However, adsorption capacity of the ZDM-NIPs was lower than that of the ZDM-MIPs. These differences suggested that few recognition sites existed on the surfaces of ZDM-NIPs. For a better understanding of the kinetic mechanisms of the adsorption process, the pseudo-first-order rate kinetic model and pseudo-second-order kinetic model (eqn (2) and (3)) were used to fit the kinetic data:

$$\text{Pseudo-first-order: } \ln(Q_e - Q_t) = \ln Q_e - K_1 t \quad (2)$$

$$\text{Pseudo-second-order: } t/Q_t = t/Q_e + 1/Q_e^2 K_2 \quad (3)$$

where  $K_1$  ( $\text{min}^{-1}$ ) and  $K_2$  ( $\text{g mg}^{-1} \text{min}^{-1}$ ) represent the pseudo-first-order rate constant and pseudo-second-order rate, respectively, and  $t$  is the adsorption time.  $Q_e$  and  $Q_t$  are the maximum adsorption amount and the adsorption amount at time  $t$ . The corresponding parameters and  $R^2$  were calculated (Table S1†). The results (Table S2†) revealed that the pseudo-second-order kinetics model ( $R_{\text{ZDM-MIPs}}^2 = 0.999$  and  $R_{\text{ZDM-NIPs}}^2 = 0.999$ ) was better fitted than the pseudo-first-order kinetics model ( $R_{\text{ZDM-MIPs}}^2 = 0.899$  and  $R_{\text{ZDM-NIPs}}^2 = 0.715$ ), which indicated the adsorption process of ASP on ZDM-MIPs/ZDM-NIPs was controlled by chemical reactions.<sup>39</sup> Fig. 4B showed the pseudo-second-order model of the equilibrium data.

**3.3.2 Adsorption isotherms.** Adsorption isotherms were investigated with different concentrations of ASP ( $10\text{--}300 \mu\text{g mL}^{-1}$ ) for ZDM-MIPs and ZDM-NIPs. As shown in Fig. 4C, the adsorption amounts of ZDM-MIPs and ZDM-NIPs increased with ASP concentration until equilibrium was reached. With increasing initial concentrations, the adsorption capacity of ZDM-MIPs increased rapidly, reaching a maximum value at  $100 \mu\text{g mL}^{-1}$  of ASP. The maximum adsorption capacity of ZDM-MIPs and ZDM-NIPs was  $13.18$  and  $9.98 \text{ mg g}^{-1}$ , respectively. Compared with ZDM-NIPs, ZDM-MIPs exhibited much higher ASP adsorption capacity, which indicated that ZDM-MIPs possessed abundant binding sites, thereby ensuring the selective recognition of ASP. The adsorption capacity of ZDM-MIPs for ASP was higher than that reported in other literatures.<sup>40,41</sup> The results also indicated the existence of specific recognition sites on the molecularly imprinted layer in ZDM-MIPs, thus

resulting in substantial specific adsorption capacity for the template ASP.

To further examine the equilibrium adsorption, we applied Langmuir and Freundlich models to describe the adsorption process. The Langmuir and Freundlich equations are as follows:

$$\text{Langmuir model: } 1/Q_e = 1/(K_L C_e Q_m) + 1/Q_m \quad (4)$$

$$\text{Freundlich model: } \log Q_e = m \log C_e + \log K_F \quad (5)$$

where  $K_L$  is the Langmuir constant, and  $K_F$  and  $m$  are the Freundlich constant.  $Q_m$  and  $Q_e$  represent the maximum adsorption amount and the adsorption amount at  $C_e$ , the concentration of ASP. As shown in Table S2,† the Langmuir model of ZDM-MIPs fitted the equilibrium data better ( $R^2 = 0.999$ ) than the Freundlich model of ZDM-MIPs ( $R^2 = 0.998$ ). The Langmuir model supposes that monolayer adsorption occurs on the adsorbent surface, while the Freundlich model is suitable for monolayer adsorption and multilayer adsorption. The findings may indicate that the adsorption process was monolayer adsorption and that the adsorption material surface was homogeneous.<sup>42</sup> Fig. 4D showed the regression curves of the Langmuir models for ZDM-MIPs and ZDM-NIPs.

### 3.4 Selectivity of ZDM-MIPs

To further investigate the selectivity of ZDM-MIPs, glycyrrhizin acid and acesulfame were selected as analogs of ASP. As shown in Fig. 4E, the binding capacity of ZDM-MIPs for ASP ( $10.01 \text{ mg g}^{-1}$ ) was 6.41 times that of glycyrrhizin acid ( $1.56 \text{ mg g}^{-1}$ ) and 6.14 times that of acesulfame ( $1.63 \text{ mg g}^{-1}$ ), thus indicating the presence of special spatial structures in ZDM-MIPs. Furthermore, the other two parameters, the imprinting factor ( $\alpha$ ) and selectivity factor ( $\beta$ ), were selected to evaluate the specificity of the adsorption capacity of ZDM-MIPs:

$$\alpha = Q_{\text{MMIP}}/Q_{\text{MNIP}} \quad (6)$$

$$\beta = \alpha_{\text{tem}}/\alpha_{\text{ana}} \quad (7)$$

where  $Q_{\text{MMIP}}$  and  $Q_{\text{MNIP}}$  are the adsorption capacity of ZDM-MIPs and ZDM-NIPs, respectively, and  $\alpha_{\text{tem}}$  and  $\alpha_{\text{ana}}$  are the

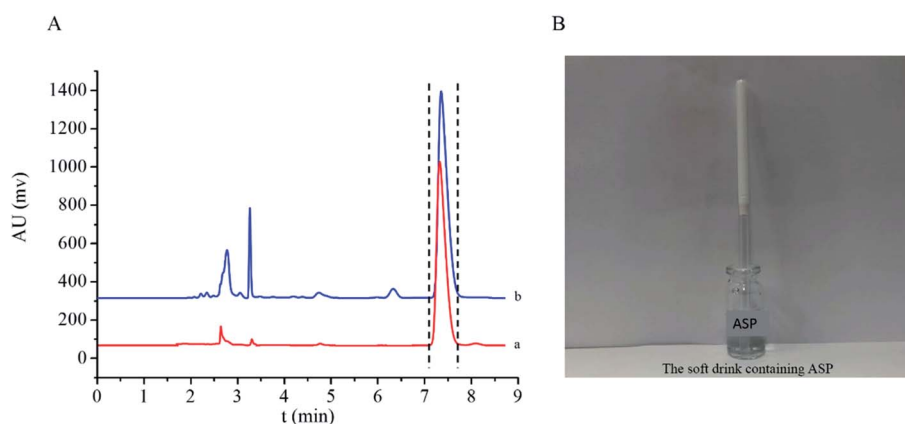


Fig. 5 (A) Chromatogram of remove ASP from soft drinks and (B) the protection sucker.



imprinting factors for the template and analogues, respectively. The imprinting factors were calculated as 4.95, 1.13, and 1.36 for ASP, glycyrrhizin acid and acesulfame, respectively. The selectivity factors were calculated as 4.38 and 3.64 for glycyrrhizin acid and acesulfame, respectively. The selectivity of ZDM-MIPs to aspartame was higher than that reported in other literatures.<sup>41,43</sup> The above results (Table S3†) showed that the prepared ZDM-MIPs had good selectivity for ASP.

### 3.5. Application of ZDM-MIPs in a real sample

**3.5.1 Removal of ASP in commercial soft drinks.** In this experiment, a health protection sucker (Fig. 5) was prepared to remove toxic levels of ASP from commercial soft drinks. The chromatograms were shown in Fig. 5A. In the figure, the curve *b* represented the chromatogram peak of the soft drink solution before the adsorption of ASP. The curve *a* represented the chromatographic peak of the soft drink solution after the adsorption of ASP. At 7.37 min, the liquid chromatographic peak of ASP appeared. The chromatographic peak of ASP (curve *a*) was clearly significantly decreased through use of the health protection aspirator. The aspirator was filled with ZDM-MIPs materials, which could adsorb and filter ASP from the soft drinks, thus providing a foundation for broad practical applications of ZDM-MIPs materials.

**3.5.2 Determination of ASP with a ZDM-MIPs-MGCE sensor.** We applied CV and DPV to investigate the electrochemical behaviors of different modified electrodes fabricated in this study. Cyclic voltammetry for the different electrodes in the redox probe solution were shown in Fig. 6A. Compared with

MGCE (curve *a*), the peak current of ZDM-MIPs-MGCE (curve *c*) increased greatly, which was attributed to the good electrical conductivity and high surface area of the ZDM-MIPs nano-composites. After adsorption of ASP, the peak current decreased (curve *b*). This decreasing trend was probably due to the ASP molecules occupying the molecularly imprinted binding sites, thereby preventing the redox reaction of the probe on the electrode surface. Fig. 6B showed the data collected with increasing concentrations of ASP. DPV curves were recorded in the range of 0.1–50  $\mu\text{g mL}^{-1}$ . For ASP, a linear relationship has been established between *I<sub>p</sub>* and analyte concentration. The current value corresponding to each concentration was the average of three measurements. The obtained linear expression was shown in Fig. 6C, and the correlation coefficient  $R^2$  was 0.9997. The modified electrode showed a good linear relationship.

**3.5.3 Applicability and accuracy of the ZDM-MIPs-MGCE sensor.** DPV experiments were performed under optimal experimental conditions. The results were shown in Table 1.

Table 1 Recovery of ASP in drink samples determined using the ZDM-MIPs-MGCE sensor ( $\pm$ RSD,  $n = 3$ )

Samples	Spiked level ( $\mu\text{g mL}^{-1}$ )	Found level ( $\mu\text{g mL}^{-1}$ )	Recovery (%)	RSD (%)
Drink	10	10.704	107.04	3.75
	20	16.982	84.91	3.55
	50	50.556	101.11	3.69

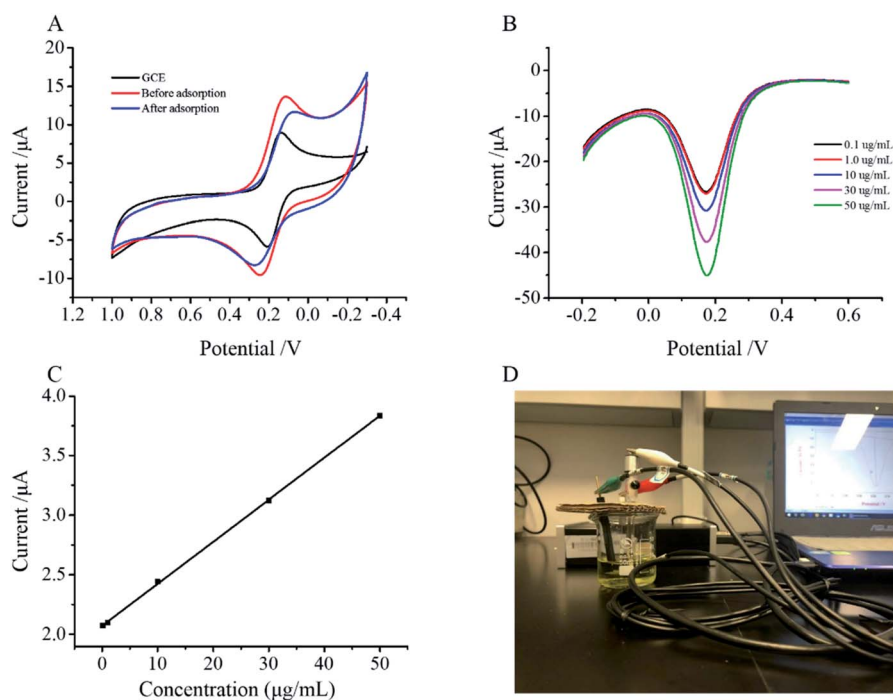


Fig. 6 (A) Cyclic voltammograms of different electrodes in the characterization solution, (B) differential pulse voltammograms of the different concentration aspartame standard solutions, (C) linear curve of aspartame standard solution, and (D) the portable electrochemical detection station.



The recoveries ranged from 84.94% to 107.04% with RSDs below 4.0%, thus indicating that the ZDM-MIPs-MGCE sensor systems had good accuracy and precision. The results suggested that the method could be used to quickly and sensitively detect concentrations of ASP in real samples.

## 4. Conclusions

In the present work, ZDM-MIPs were synthesized to recognize and enrich ASP in real samples. The results of SEM, TEM, and FT-IR demonstrated that the core-shell structure of ZDM-MIPs was synthesized successfully. The TGA, VSM, and XRD results indicated good thermal stability and excellent magnetic response of ZDM-MIPs. Adsorption experiments showed that ZDM-MIPs had excellent adsorption capacity ( $12.86 \text{ mg g}^{-1}$ ) at 60 min. The DPV and CV results demonstrated that the modified MGCE had a good electrochemical response. A portable electrochemical detection station was used in this experiment. Furthermore, the sensor systems demonstrated good accuracy and precision, with recovery percentages between 84% and 107%. The ZDM-MIPs developed in this study could be used to remove ASP from beverages and determine the ASP content quickly and easily in test samples, thereby providing a solid theoretical basis for applications in the food and pharmaceutical industries.

## Conflicts of interest

The authors declare no conflict of interest.

## Acknowledgements

This work was supported by National Natural Science Foundation of China (Grant No. 81973451); Fundamental Research Funds for the Central Universities (Grant No. 2019CDYGYB027, 2019CDXYHG0013 and 2017CDJXFLX0014); Fundamental and Frontier Research Fund of Chongqing (Grant No. cstc2019jsjy-zysbAX0020 and No. cstc2018jcjyAX0661); Science and Technology Research Program of Chongqing Municipal Education Commission (Grant No. KJZD-K201800103); Graduate Research and Innovation Foundation of Chongqing, China (Grant No. CYS18033); Venture & Innovation Support Program for Chongqing Overseas Returnees, and Tang Foundations.

## References

- 1 P. C. G. Magalhaes, R. Abadie-Guedes, M. A. B. da Costa Mendonca, A. D. de Souza and R. C. A. Guedes, Behavioral and electrophysiological brain effects of aspartame on well-nourished and malnourished rats, *Metab. Brain Dis.*, 2019, **34**, 651–658.
- 2 A. D. Mooradian, M. Smith and M. Tokuda, The role of artificial and natural sweeteners in reducing the consumption of table sugar: a narrative review, *Clinical Nutrition ESPEN*, 2017, **18**, 1–8.
- 3 A. M. Shalaby, M. Ibrahim and A. M. Aboregela, Effect of aspartame on the placenta of adult albino rat. A histological and immunohistochemical study, *Ann. Anat.*, 2019, **224**, 133–141.
- 4 M. Soffritti, F. Belpoggi, M. Manservigi, E. Tibaldi, M. Lauriola, L. Falcioni and L. Bua, Aspartame administered in feed, beginning prenatally through life span, induces cancers of the liver and lung in male Swiss mice, *Am. J. Ind. Med.*, 2010, **53**, 1197–1206.
- 5 D. S. Wikoff, G. A. Chappell, S. Fitch, C. L. Doeppker and S. J. Borghoff, Lack of potential carcinogenicity for aspartame – systematic evaluation and integration of mechanistic data into the totality of the evidence, *Food Chem. Toxicol.*, 2020, **135**, 110866.
- 6 A. V. T. Le, Y. L. Su and S. H. Cheng, A novel electrochemical assay for aspartame determination *via* nucleophilic reactions with caffeic acid ortho-quinone, *Electrochim. Acta*, 2019, **300**, 67–76.
- 7 C. Cheng and S. C. Wu, Simultaneous analysis of aspartame and its hydrolysis products of Coca-Cola Zero by on-line postcolumn derivation fluorescence detection and ultraviolet detection coupled two-dimensional high-performance liquid chromatography, *J. Chromatogr. A*, 2011, **1218**, 2976–2983.
- 8 X. Li, S. Li, H. Li, J. Wang, Q. Luo and X. Yin, Quantification of artificial sweeteners in alcoholic drinks using direct analysis in real-time QTRAP mass spectrometry, *Food Chem.*, 2021, **342**, 128331.
- 9 J. W. Xu, Z. M. Cui, Z. Q. Liu, F. Xu, Y. S. Chen and Y. L. Luo, Organic-Inorganic Nanohybrid Electrochemical Sensors from Multi-Walled Carbon Nanotubes Decorated with Zinc Oxide Nanoparticles and *In Situ* Wrapped with Poly(2-methacryloyloxyethyl ferrocenecarboxylate) for Detection of the Content of Food Additives, *Nanomaterials*, 2019, **9**, 1388–1407.
- 10 J. G. Pacheco, M. S. V. Silva, M. Freitas, H. P. A. Nouws and C. Delerue-Matos, Molecularly imprinted electrochemical sensor for the point-of-care detection of a breast cancer biomarker (CA 15-3), *Sens. Actuators, B*, 2018, **256**, 905–912.
- 11 M. A. Beluomini, J. L. da Silva, A. C. de Sá, E. Buffon, T. C. Pereira and N. R. Stradiotto, Electrochemical sensors based on molecularly imprinted polymer on nanostructured carbon materials: a review, *J. Electroanal. Chem.*, 2019, **840**, 343–366.
- 12 M. Baghayeri, H. Alinezhad, M. Fayazi, M. Tarahomi, R. Ghanei-Motlagh and B. Maleki, A novel electrochemical sensor based on a glassy carbon electrode modified with dendrimer functionalized magnetic graphene oxide for simultaneous determination of trace Pb(II) and Cd(II), *Electrochim. Acta*, 2019, **312**, 80–88.
- 13 R.-R. Zhang, J. Zhan, J.-J. Xu, J.-Y. Chai, Z.-M. Zhang, A.-L. Sun, J. Chen and X.-Z. Shi, Application of a novel electrochemiluminescence sensor based on magnetic glassy carbon electrode modified with molecularly imprinted polymers for sensitive monitoring of bisphenol A in seawater and fish samples, *Sens. Actuators, B*, 2020, **317**, 128237.
- 14 M. Baghayeri, H. Veisi and M. Ghanei-Motlagh, Amperometric glucose biosensor based on immobilization



- of glucose oxidase on a magnetic glassy carbon electrode modified with a novel magnetic nanocomposite, *Sens. Actuators, B*, 2017, **249**, 321–330.
- 15 W. Guo, J. Ma, X. Cao, X. Tong, F. Liu, Y. Liu, Z. Zhang and S. Liu, Amperometric sensing of hydrazine using a magnetic glassy carbon electrode modified with a ternary composite prepared from Prussian blue, Fe<sub>3</sub>O<sub>4</sub> nanoparticles, and reduced graphene oxide, *Microchim. Acta*, 2017, **184**, 3163–3170.
  - 16 J. P. Fan, J. X. Yu, X. M. Yang, X. H. Zhang, T. T. Yuan and H. L. Peng, Preparation, characterization, and application of multiple stimuli-responsive rattle-type magnetic hollow molecular imprinted poly (ionic liquids) nanospheres (Fe<sub>3</sub>O<sub>4</sub>@void@PILMIP) for specific recognition of protein, *Chem. Eng. J.*, 2018, **337**, 722–732.
  - 17 F. A. Ishkuh, M. Javanbakht, M. Esfandiyari-Manesh, R. Dinarvand and F. Atyabi, Synthesis and characterization of paclitaxel-imprinted nanoparticles for recognition and controlled release of an anticancer drug, *J. Mater. Sci.*, 2014, **49**, 6343–6352.
  - 18 Y. Ge, P. Guo, X. Xu, G. Chen, X. Zhang, H. Shu, B. Zhang, Z. Luo, C. Chang and Q. Fu, Selective analysis of aristolochic acid I in herbal medicines by dummy molecularly imprinted solid-phase extraction and HPLC, *J. Sep. Sci.*, 2017, **40**, 2791–2799.
  - 19 Z. Wu, D. He, B. Cui and Z. Jin, Ultrasensitive detection of microcystin-LR with gold immunochromatographic assay assisted by a molecular imprinting technique, *Food Chem.*, 2019, **283**, 517–521.
  - 20 S. Xu, H. Lu, J. Li, X. Song, A. Wang, L. Chen and S. Han, Dummy molecularly imprinted polymers-capped CdTe quantum dots for the fluorescent sensing of 2,4,6-trinitrotoluene, *ACS Appl. Mater. Interfaces*, 2013, **5**, 8146–8154.
  - 21 E. Shoghi, S. Z. Mirahmadi-Zare, R. Ghasemi, M. Asghari, M. Poorebrahim and M. H. Nasr-Esfahani, Nanosized aptameric cavities imprinted on the surface of magnetic nanoparticles for high-throughput protein recognition, *Mikrochim. Acta*, 2018, **185**, 241.
  - 22 S. Hua, L. Zhao, L. Cao, X. Wang, J. Gao and C. Xu, Fabrication and evaluation of hollow surface molecularly imprinted polymer for rapid and selective adsorption of dibenzothiophene, *Chem. Eng. J.*, 2018, **345**, 414–424.
  - 23 V. M. A. Mohanan, A. K. Kunnummal and V. M. N. Biju, Selective electrochemical detection of dopamine based on molecularly imprinted poly(5-amino 8-hydroxy quinoline) immobilized reduced graphene oxide, *J. Mater. Sci.*, 2018, **53**, 10627–10639.
  - 24 P. He, H. Zhu, Y. Ma, N. Liu, X. Niu, M. Wei and J. Pan, Rational design and fabrication of surface molecularly imprinted polymers based on multi-boronic acid sites for selective capture glycoproteins, *Chem. Eng. J.*, 2019, **367**, 55–63.
  - 25 Z. Zhang, D. Niu, Y. Li and J. Shi, Magnetic, core-shell structured and surface molecularly imprinted polymers for the rapid and selective recognition of salicylic acid from aqueous solutions, *Appl. Surf. Sci.*, 2018, **435**, 178–186.
  - 26 Y. Fu, Z. You, A. Xiao and L. Liu, Magnetic molecularly imprinting polymers, reduced graphene oxide, and zeolitic imidazolate frameworks modified electrochemical sensor for the selective and sensitive detection of catechin, *Microchim. Acta*, 2021, **188**, 71.
  - 27 W. Xu, Y. Wang, X. Wei, J. Chen, P. Xu, R. Ni, J. Meng and Y. Zhou, Fabrication of magnetic polymers based on deep eutectic solvent for separation of bovine hemoglobin via molecular imprinting technology, *Anal. Chim. Acta*, 2019, **1048**, 1–11.
  - 28 C. Z. Gomez-Castro, J. A. Rodriguez, J. Cruz-Borbolla, A. Quintanar-Guzman, I. Sanchez-Ortega and E. M. Santos, A theoretical and experimental approach to evaluate zein-calcium interaction in nixtamalization process, *Food Chem.*, 2019, **297**, 124995.
  - 29 B. Zhang, Y. Luo and Q. Wang, Effect of acid and base treatments on structural, rheological, and antioxidant properties of  $\alpha$ -zein, *Food Chem.*, 2011, **124**, 210–220.
  - 30 Q. Zhong and M. Jin, Zein nanoparticles produced by liquid-liquid dispersion, *Food Hydrocolloids*, 2009, **23**, 2380–2387.
  - 31 A. G. Ayankojo, J. Reut, A. Opik, A. Furchner and V. Syrtiski, Hybrid molecularly imprinted polymer for amoxicillin detection, *Biosens. Bioelectron.*, 2018, **118**, 102–107.
  - 32 M. Baghayeri, M. Rouhi, M. M. Lakouraj and M. Amiri-Aref, Bioelectrocatalysis of hydrogen peroxide based on immobilized hemoglobin onto glassy carbon electrode modified with magnetic poly(indole-co-thiophene) nanocomposite, *J. Electroanal. Chem.*, 2017, **784**, 69–76.
  - 33 J. W. Zhang, L. Tan, Y. Z. Zhang, G. C. Zheng, Z. N. Xia, C. Z. Wang, L. D. Zhou, Q. H. Zhang and C. S. Yuan, Debitting of lemon juice using surface molecularly imprinted polymers and the utilization of limonin, *J. Chromatogr. B: Anal. Technol. Biomed. Life Sci.*, 2019, **1104**, 205–211.
  - 34 X. Fu, D. Zhu, L. Huang, X. Yan, S. Liu and C. Wang, Superparamagnetic core-shell dummy template molecularly imprinted polymer for magnetic solid-phase extraction of food additives prior to the determination by HPLC, *Microchem. J.*, 2019, **150**, 104169.
  - 35 S. Dong, X. y. Li, P. Guo, Y. Chen and H. j. Li, Preparation and characterization of PCL-grafted zein film via atmospheric-pressure cold plasma pretreatment, *Plasma Processes Polym.*, 2021, e2000242.
  - 36 S. Chen, Q. Li, D. J. McClements, Y. Han, L. Dai, L. Mao and Y. Gao, Co-delivery of curcumin and piperine in zein-carrageenan core-shell nanoparticles: formation, structure, stability and *in vitro* gastrointestinal digestion, *Food Hydrocolloids*, 2020, **99**, 105334.
  - 37 H. Asadi, A. Ghaee, J. Nourmohammadi and A. Mashak, Electrospun zein/graphene oxide nanosheet composite nanofibers with controlled drug release as antibacterial wound dressing, *Int. J. Polym. Mater. Polym. Biomater.*, 2019, **69**, 173–185.
  - 38 Z. Liu, Y. Wang, F. Xu, X. Wei, J. Chen, H. Li, X. He and Y. Zhou, A new magnetic molecularly imprinted polymer based on deep eutectic solvents as functional monomer



- and cross-linker for specific recognition of bovine hemoglobin, *Anal. Chim. Acta*, 2020, **1129**, 49–59.
- 39 Y. Zhao, D. Du, Q. Li, W. Chen, Q. Li, Q. Zhang and N. Liang, Dummy-surface molecularly imprinted polymers based on magnetic graphene oxide for selective extraction and quantification of pyrethroids pesticides in fruit juices, *Microchem. J.*, 2020, **159**, 105411.
- 40 S. Zhao, X. Yang, H. Zhao, A. Dong, J. Wang, M. Zhang and W. Huang, Water-compatible surface imprinting of 'Saccharin sodium' on silica surface for selective recognition and detection in aqueous solution, *Talanta*, 2015, **144**, 717–725.
- 41 M. Singh, A. Kumar and N. Tarannum, Water-compatible 'aspartame'-imprinted polymer grafted on silica surface for selective recognition in aqueous solution, *Anal. Bioanal. Chem.*, 2013, **405**, 4245–4252.
- 42 Y. Sun and W. Zheng, Surface molecular imprinting on polystyrene resin for selective adsorption of 4-hydroxybenzoic acid, *Chemosphere*, 2021, **269**, 128762.
- 43 J. Srivastava, N. Gupta, A. Kushwaha, S. Umrao, A. Srivastava and M. Singh, Highly sensitive and selective estimation of aspartame by chitosan nanoparticles-graphene nanocomposite tailored EQCM-MIP sensor, *Polym. Bull.*, 2018, **76**, 4431–4449.

